Characterization of a precast hemp concrete block. Part II: Hygric properties

Billy Seng, Camille Magniont, Sylvie Lorente

Characterization of a precast hemp concrete block. Part II: Hygric properties

Billy SENG, Camille MAGNIONT, Sylvie LORENTE

LMDC, Université de Toulouse, UPS, INSA, 135 Avenue de Rangueil, 31077 Toulouse cedex 04, France

Corresponding author: Camille MAGNIONT

e-mail: camille.magniont@insa-toulouse.fr

Abstract

The hygroscopic, insulating and agronomic properties of hemp concrete make it a promising building material for addressing the sustainable building challenge. Part I of this series of two papers described a characterization of the thermal properties of a prefabricated hemp concrete block, confronting the impact of different methods of measurement. Part II focuses on the hygric properties, which describe moisture transfer and storage. The sorption isotherm was measured at 23 °C and 45 °C, considering distinct experimental procedures (saturation salt solution (SSS) methods with single relative humidity step or stepwise equilibrium, and Dynamic Vapour Sorption (DVS)). Differences were observed in the results and hypotheses are formulated considering the distinct drying procedures between SSS and DVS methods or the specific water vapour sorption process on cellulose-based materials. With the measurements at two temperatures, the isosteric heat of sorption is evaluated which allows an evaluation of the sorption at any temperature. The water vapour permeability was measured with dry and wet cups. Different parameters were tested: thickness (5 and 8 cm), air velocity (0.5 and 2 $m.s^{-1}$) and calculation method (standard calculations, consideration of the water vapour interface resistances). Each parameter, with the chosen values, had an impact of around 10% on the final water vapour permeability calculated. The capillary absorption coefficient was evaluated through capillary uptake measurements, leading to an estimation of the liquid transfer coefficient, albeit 12 times lower than the one evaluated thanks to the dry and wet water vapour permeabilities. All these observations underline the significant impact of experimental parameters and methods on the determination of hemp concrete hygric properties and support the necessity to develop more specific measurement methods for such permeable and hygroscopic bio-based building materials.

Keywords: Hygric properties, water vapour permeability, sorption isotherm, capillary absorption.

NOMENCLATURE

Latin symbols

A	area	(m^2)
A_w	capillary absorption coefficient	$(kg.m^{-2}.s^{-1/2})$
c_p	specific heat capacity	$(J.kg^{-1}.K^{-1})$
d	thickness	(m)
D_w	liquid transfer coefficient	$(m^2.s^{-1})$
g_v	vapour flux density	$(kg.m^{-2}.s^{-1})$
h_c	convective heat transfer coefficient	$(W.m^{-2}.K^{-1})$
h_m	mass transfer coefficient	$(kg.m^{-2}.s^{-1}.Pa^{-1})$
Le	Lewis number	(-)
m	mass	(kg)
M_w	water molar mass	$(kg.mol^{-1})$
p_v	water vapour pressure	(Pa)
$p_{v,sat}$	saturation water vapour pressure	(Pa)
q_{st}	isosteric heat of sorption	$(J.kg^{-1})$
R	gas constant	$(J.kg^{-1}.K^{-1})$
T	temperature	(K)
t	time of absorption	(s)
u	moisture content	$(kg.kg^{-1})$
v	velocity	$(m.s^{-1})$
w	volumetric moisture content	$(kg.m^{-3})$
Z	water vapour resistance	$(m^2.s.Pa.kg^{-1})$

Greek symbols

δ_v	water vapour permeability	($kg.m^{-1}.s^{-1}.Pa^{-1}$)
μ	water vapour resistance factor	(-)
ξ_{RH}	moisture capacity	($kg.m^{-3}$)
ρ	density	($kg.m^{-3}$)

Subscripts

$_0$	dry state
$_{air}$	air
$_f$	free saturation
$_{int}$	interface
$_m$	monolayer sorption
$_{mat}$	material
$_v$	vapour

1. Introduction

The building sector is responsible for major environmental impacts, mainly in terms of consumption of non-renewable raw materials, emission of greenhouse gases and waste production. The design and characterization of innovative eco-friendly building materials has thus become a priority. The use of bio-based raw materials could be a response to this environmental challenge as bio-based aggregates are renewable, mainly by-products of local crops, and contribute to the reduction of buildings climate impacts (Peñaloza et al., 2016). Over the last fifteen years, these environmental benefits have contributed to the development of a specific building material commonly called hemp concrete, lime-hemp, hemp lime or hempcrete. This composite combines a mineral binder, generally based on lime and possibly including pozzolanic additions, and a plant aggregate: hemp shiv, extracted from the hemp stalk by a mechanical defibration process.

Numerous scientific studies have shown the efficient insulating and hygroscopic properties of hemp concrete. However, one of the main disadvantages of hemp shiv aggregate is its high water absorption rate, which generates the need for an excessive amount of water at the time of mixing and, consequently, a very long drying time, unsuitable for modern construction. In this context, previous works (Escadeillas et al., 2010; Gazagnes et al., 2010) led to the development of hemp concrete blocks produced using a vibro-compaction process at industrial scale by the SEAC company, France.

The first paper of this series focused on the characterization of these precast hemp concrete blocks in terms of physical and thermal performance. In this second paper, the emphasis will be on the hygric properties. The characterization of this material is performed in order to simulate its hygrothermal behaviour in a further study using a heat and moisture model presented by Seng et al. (2017) and to confront these results with experimental data obtained at wall scale from a bi-climatic chamber (Vu et al., 2015).

The hygric experimental characterization of hemp concrete is still open to discussion. Thus, depending on the author, the chosen parameter and/or the method of measurement can differ. For example, when tackling the high range of humidity, there are several ways to describe the moisture transfer phenomena. Nevertheless, since hemp concrete is not a structural building material, it is designed to fill a timber frame and to be protected from liquid water by exterior cladding and capillary barrier. Consequently, under normal use, hemp concrete should not be submitted to very high humidity. The hygric properties commonly studied in the literature on biobased building materials are thus the sorption isotherm, the water vapour permeability and sometimes a value based on capillary uptake.

The sorption isotherm is generally measured based on NF EN ISO 12571 (AFNOR, 2013) with saturated salt solutions or a climatic chamber (Collet et al., 2013; de Bruijn and Johansson, 2013; Mazhoud et al., 2016; Rahim et al., 2016a). This protocol is well established, even though the approach is time consuming. Ongoing research in experimental measurement and numerical modelling focuses on reducing the measurement time, the consideration of hysteresis and the impact of temperature. Feng et al. (2015) made an advanced study suggesting that the effect of temperature is not consistent. Moreover, the impact can be confused or drowned by the experimental errors of the measuring apparatus. The study by Feng et al. (2015) was performed on mineral materials only. In contrast, recent studies based on bio-sourced materials have underlined the need to take the temperature effect into account for good prediction of sorption behaviour (Aït Oumeziane et al., 2016; Colinart and Glouannec, 2017; Rahim et al., 2016b). Colinart and Glouannec (2017) compared the results of autoclaved aerated concrete, hemp concrete and wood fibre insulation. In spite of measurement uncertainties, they showed that the influence of temperature is accentuated for bio-sourced material. Aït Oumeziane et al. (2016) observed that the impact of temperature is particularly noteworthy when hysteresis phenomena are taken into account. Alternative

measurement methods have emerged for studying the sorption of building materials, such as the dynamic vapour sorption method. This has been used by Latif et al. (2015), for example. Nevertheless, this technique is questionable given the limited size of the sample and the great heterogeneity of hemp concrete. The measurements obtained with these two techniques will be compared in the present article.

The water vapour permeability is measured according to standards such as NF EN ISO 12572 (AFNOR, 2001), using the “cup method” with a difference of relative humidity across a sample. Some questions have emerged concerning the case of permeable materials, namely on the influence of the air layer in the cup. Recently, a new approach has been proposed for evaluating the water vapour resistance of the air layer in the latest version of standard NF EN ISO 12572 (AFNOR, 2016). Another axis of research deals with the surface resistance, i.e. the resistance of the air at the top of the cup. NF EN ISO 12572 (AFNOR, 2016) points out that it can be neglected when the air velocity is sufficient, i.e. at least at 2 $m.s^{-1}$. This hypothesis was investigated by some authors, e.g. Vololonirina et al. (2014). The literature rarely indicates whether both the air layer and surface resistances are considered, except in the works of Rahim et al. (2016) who took account of the air layer vapour resistance as well as the surface vapour resistance. Other authors have expressed the vapour permeability as a function of the RH. This approach was chosen by Collet et al. (2013), for example.

When considering the capillary condensation region, the description method of the moisture transfer phenomena remains varied. Some authors use the water vapour permeability in the full moisture range or use the water vapour permeability assessed by the wet-cup method to determine a liquid transfer coefficient in the hygroscopic region (Künzel, 1995). Others rely on measurements based on capillary uptake. Advanced techniques allow precise observation of the moisture profile over time (Roels et al., 2004): gamma-ray attenuation, neutron radiography or NMR techniques. However, these studies are heavy and require expensive

apparatus. Another, easier approach uses a gravimetric method, resulting in the expression of a capillary absorption coefficient A_w ($kg.m^{-2}.s^{-1/2}$), regulated by a standard or equivalent, such as the one presented by Arliguie and Hornain (2007).

The present paper aims to characterize the hygric properties of a precast hemp concrete (water vapour permeability, liquid transfer coefficient and sorption isotherms). All the measurements are made on samples directly extracted from the industrially produced bricks. Therefore, the large variability of performance often reported in the literature due to the manual casting method is limited. The second objective of the present study is to investigate the impact of the experimental methods and protocols on the assessed performances. When possible, different methods are used to measure the same parameter and the results are compared to the literature, where “homemade” protocols or non-specific standards have often been applied.

2. Material and methods

2.1. Material

The material we are interested in came from SEAC, a company specializing in concrete walls and floors, and also developing sustainable construction materials. The design of the brick was the result of previous research works on the material formulation, performed jointly by SEAC and LMDC, and which led to two patents for a vibro-compacted precast hemp concrete (HC) (Escadeillas et al., 2010; Gazagnes et al., 2010). The precast block was made of hemp shiv aggregates and an innovative lime-metakaolin (LM) binder (Dinh et al., 2015; Magniont et al., 2012).

The hemp shiv aggregates are ligneous particles extracted from the core of hemp stems (Cannabis sativa) through an industrial defibration process using mechanical breaking. The particles are then dusted and calibrated. The pozzolanic matrix was made of lime and metakaolin, produced by flash calcination of kaolinite at 700 °C, and mainly composed of amorphous silicon-aluminates and quartz.

The precast block, previously cured in the prefabrication plant, can be used directly on a construction site without a long drying time. However, the material is not a load-bearing construction product, and it needs a framework such as a post and beam structure. At present, the bricks are intended to be used as filling material only. In Figure 1, two types of block are presented. Type B block, with an empty space, allows for the passage of the load-bearing structure. In this study, we focus on type A bricks.

Figure 1: Type A brick (left) and type B brick (right) for framework post

As presented (Seng et al., 2018), the apparent density of the HC is 466 ±25 kg.m^{-3} with a total porosity of 0.78 ±0.04, most of which corresponds to the open porosity (0.76 ±0.01).

For the different experiments, samples were cut from the slabs of the bricks with a circular bridge saw for rectangular samples and with a core drilling machine for cylindrical samples. The dimensions of the samples are given in Table 1. In order to avoid shredding, the cutting lines on the samples were soaked with water prior to the cutting process. All the samples were taken off in such a way that the studied transfer was in the same direction, i.e. along the horizontal axis of the brick, even for capillary water absorption.

Parameter studied	Geometry – Dimensions	Balance /precision	
Sorption isotherm (Saturated salt solution)	Rectangular 60x100x25mm^3	Precisa XT 620M	10^{-3} g
Sorption isotherm (Dynamic Vapour Sorption)	Few hundred mg	-	-

Water vapour permeability	Cylindrical: radius=110 mm, height=25 mm	Precisa XT 620M	10^{-3} g
Capillary water absorption coefficient	Rectangular 100x60x30 mm^3	Sartorius LP 620 P	10^{-3} g

Table 1: Samples geometry and balance information for weight stabilization monitoring and experimental study

2.2. Methods

Prior to the measurement, all the samples were dried in an oven at 50 °C for saturated salt solution sorption, water vapour permeability and capillary water uptake measurement. For the water vapour permeability measurement, the samples were placed in equilibrium in a climatic chamber (WEISS WK3-2000) at 23 °C and 50% RH. The drying and the equilibrium with the surroundings were considered to be achieved when the sample mass change was less than 0.1% between three weighings at least 24 hours apart (5% for the vapour permeability equilibrium study). A specific drying process was applied for dynamic vapour sorption measurement.

All the measurements in this paper were gravimetric methods. The balances used and their precisions are presented in Table 1.

2.2.1. Sorption isotherm

The sorption isotherm expresses the amount of moisture that a material contains when in equilibrium with its environment. It is characterized by the moisture content u ($kg.kg^{-1}$ of material) or w ($kg.m^{-3}$ of material) as a function of the relative humidity (RH).

The assessment of the water vapour sorption isotherm of HC was performed with the saturated salt solutions method and by means of a Dynamic Vapour Sorption (DVS) apparatus. Both methods are detailed below.

The saturated salt solution method is based on the standard NF EN ISO 12571 (AFNOR, 2013). After drying, the samples were placed in a sealed ventilated box with a saturated salt solution that set the required relative humidity. In order to maintain the targeted temperature, all the boxes were placed in a climatic chamber set at 23 °C. Five relative humidities were investigated (Table 2). Eight samples were initially inserted into each box. In time, the samples reached mass equilibrium due to water adsorption/desorption. Equilibrium was considered to be reached when the change of mass between three consecutive weighings, at least 24 hours apart, was less than 0.1% of the total mass. The moisture content u ($kg.kg^{-1}$) was calculated according to Eq. (1):

$$u = (m - m_0)/m_0 \quad (1)$$

where m is the mass of the sample in equilibrium (kg) and m_0 is the mass of the dry sample (kg).

Saturated salt solution	Relative humidity at 23°C (NF EN ISO 12571)	Relative humidity at 45°C (NF EN ISO 12571)
Sodium hydroxide, NaOH	7.98±1.9 %	3.61±0.65%
Magnesium chloride, $MgCl_2$	32.9±0.17 %	31.10±0.13%
Sodium chloride, NaCl	75.36±0.13 %	74.52±0.16%
Potassium nitrate, KNO_3	94.00±0.60 %	87.03±1.8%
Potassium sulfate, K_2SO_4	97.42±0.47 %	96.12±0.40%

Table 2: Relative humidities and corresponding saturated salt solutions according to NF EN ISO 12571 (AFNOR, 2013)

In order to evaluate the impact of the relative humidity history applied to reach moisture equilibrium, two approaches were chosen in sorption: direct sorption from the dry state to each chosen relative humidity (single RH step), and gradual sorption from the dry state to successive relative humidities (gradual RH steps). Desorption started at the highest relative humidity (97% RH) and decreased through the different steps of relative humidity. The desorption study was performed with eight samples.

A sorption and desorption study was also performed at 45 °C. Only the gradual approach was chosen for this temperature, due to space and time constraints.

Dynamic Vapour Sorption (DVS) is also a gravimetric method, initially used in the pharmaceutical and agrofood industries. The sample of material was placed in a crucible that was continuously weighed by a microbalance. This ensemble was in a closed chamber where the temperature and relative humidity were controlled by mixing a dry gas, nitrogen, and water vapour, Figure 2.

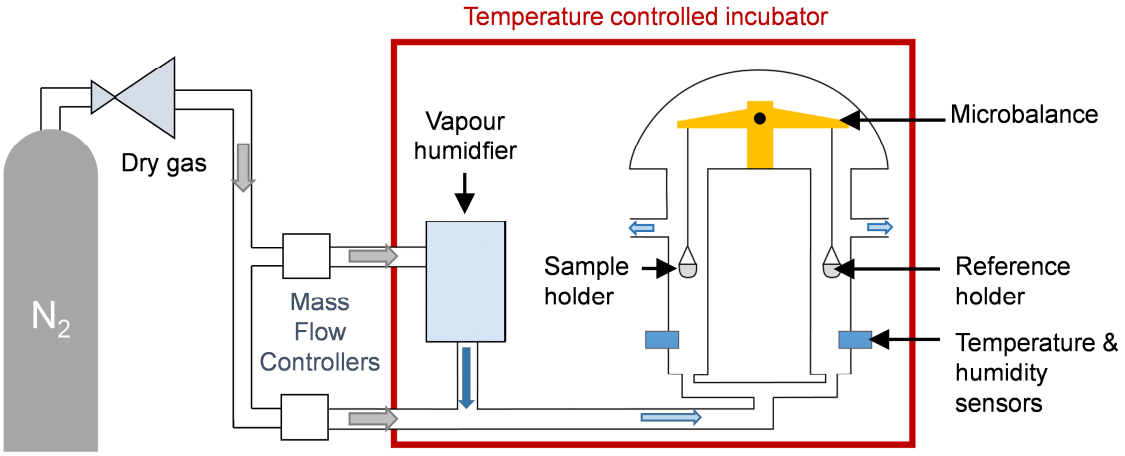

Figure 2: Scheme of the DVS device, based on (Surface Measurement Systems, 2000).

Prior to the measurement, a drying stage was performed for two hours at 50°C and about 0%RH (dry dinitrogen flush) followed by 30 minutes at 23°C and similar RH conditions. Then a sorption test was performed, by steps of 10% RH with an additional step at 95% RH. The mass of the sample was monitored continuously. The two stopping criteria were a stabilization criterion set at 10^{-4} % relative mass change per min and a duration criterion (6 hours for RH<80%, 12 h for 80%<RH<90% and 18 h for RH=95%). Two samples were tested at 23 °C. Their initial masses in the dry state were around 317 mg and 154 mg.

Many models exist for linking moisture content and relative humidity. Based on physical or mathematical considerations, they are convenient for modelling heat and moisture transfers. One of the most commonly used, the GAB model (for Guggenheim, Andersen and de Boer (Anderson, 1946)), is frequently used for describing the isotherm in a wide range of relative humidity. It is given by Eq. (2):

$$u = \frac{u_m \cdot C \cdot K \cdot RH}{(1 - K \cdot RH)(1 + K(C-1)\mathrm{RH})} \qquad (2)$$

where u_m, C and K are, respectively, the moisture content with one layer of adsorption (kg/kg), the energy coefficient dealing with multilayer and bulk liquid water, and the

coefficient dealing with monolayer and multilayer water sorption. In fact, these coefficients are chosen to fit the experimental data.

2.2.2. Vapour permeability

The water vapour permeability δ_v ($kg.m^{-1}.s^{-1}.Pa^{-1}$) is the ability of a material to allow water vapour to pass through it, under a difference of vapour pressure.

The measurement of this parameter was based on NF EN ISO 12572 (AFNOR, 2016) and used the so called cup method with saturated salt solution (SSS) (Figure 3). There are two main types of standard measurements: “dry cup” and “wet cup”. As described in NF EN ISO 12572 (AFNOR, 2016), the “dry cup” test gives information on the water vapour permeability at low relative humidities, i.e. when moisture transfer is mainly due to vapour diffusion. A “wet cup” test is performed in higher humidity conditions and accounts for both water vapour and liquid water transfers as condensation occurs in the pores. As the aim was to measure the vapour permeability here, the study focused on “dry cup” tests, described below, in which two thicknesses and two air velocities were assessed. Nevertheless, to fully characterize the material, a standard measurement was performed with “wet cup” conditions, giving a comparison point for liquid transfers with the capillary absorption coefficient test.

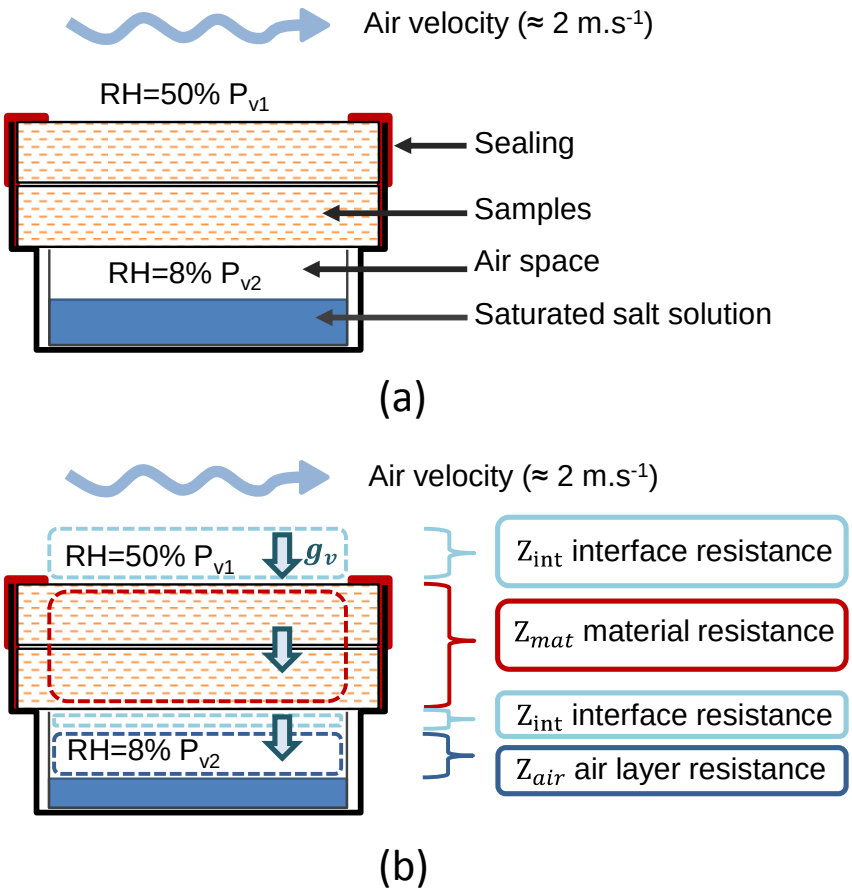

Figure 3: Scheme of the dry cup assembly for vapour permeability measurement (a) and the different water vapour resistance layers (b) (adapted from (Vololonirina and Perrin, 2016)).

For the "dry cup" measurement, a solution of saturated sodium hydroxide (NaOH) in the bottom of the aluminium cup established an inside relative humidity of around 8±2% at 23 °C. Two sample thicknesses were tested. They were made by stacking layers of hemp concrete for which the interface surfaces were sanded in order to limit the air layer. The samples were 5 cm (2 layers) and 8 cm (3 layers) thick. The cups were sealed with a mixture of wax and paraffin and put into a climatic chamber at a temperature of 23 °C and 50% RH. The air velocity above the cup was measured with a hot-wire anemometer. Two air velocities were tested for 5 cm thick samples: around 2 $m.s^{-1}$ and 0.5 $m.s^{-1}$. For "wet cup"

measurements, a solution of potassium nitrate (KNO_3) ensured an inside relative humidity of around 94±1%, and the outside environment was set at 50% RH by the climatic chamber.

The cups were regularly weighed until a steady state was reached (Precisa XT 620M (10^{-3} g) and Sartorius CPA 4202 S (10^{-2} g)), i.e. when the mass gain G ($kg.s^{-1}$) was constant, Eq. (3).

$$G = \frac{\Delta m}{\Delta t} \tag{3}$$

The vapour flux density g_v ($kg.m^{-2}.s^{-1}$) can be linked to the difference of water vapour pressure Δp_v (Pa) described by Fick's law, Eq. (4). The water vapour resistance Z_i ($m^2.s.Pa.kg^{-1}$) is defined in Eq. (5). Finally, the apparent water vapour resistance includes three main components (Eq. (6)): the interface water vapour resistance Z_{int} at the top of the material and probably between the material and the air layer, the material water vapour resistance Z_{mat}, and the water vapour resistance Z_{air} of the air layer between the material and the saturated salt solution.

$$g_v = \frac{G}{A} = \frac{1}{Z_{app}} \Delta p_v \tag{4}$$

$$Z_i = \frac{d_i}{\delta_i} \tag{5}$$

where d_i is the thickness of component i (m).

$$Z_{app} = Z_{int} + Z_{mat} + Z_{air} \tag{6}$$

The interface resistance Z_{int} is defined as the inverse of the mass transfer coefficient h_m ($kg.m^{-2}.s^{-1}.Pa^{-1}$), Eq. (7). The mass transfer coefficient h_m can be determined with the Lewis equation, based on an analogy between mass and heat transfers, Eq. (8).

$$Z_{int} = 1/h_m \tag{7}$$

$$\frac{1}{h_m} = \frac{R_v \cdot T \cdot \left(\rho c_p\right)_{air}}{h_c} \cdot Le^{\frac{3}{4}} \quad (8)$$

where R_v is the gas constant for vapour (R_v=461.5 J.kg^{-1}.K^{-1}), T is the temperature (T=293.15 K here), ρ_{air} is the air density (ρ_{air}=1.2 kg.m^{-3}), $c_{p,air}$ is the specific heat capacity of air ($c_{p,air}$= 1004 J.kg^{-1}.K^{-1}), h_c (W.m^{-2}.K^{-1}) is the convective heat transfer coefficient and Le is the Lewis number (for air/water vapour, the Lewis number is close to one). We can actually identify two mass transfer coefficients: $h_{m,in}$ inside the cup, between the air layer and the material, and $h_{m,out}$ outside the cup,

In the literature, the convective heat transfer coefficient h_c (W.m^{-2}.K^{-1}) is expressed as a function of the air velocity. Based on a literature analysis, the values given in NF EN 15026 (AFNOR, 2008), and by Hens et al. (2007), McAdams (1954) and Pedersen (1990) were chosen as they showed similar results. The corresponding mass transfer coefficients h_m (kg.m^{-2}.s^{-1}.Pa^{-1}) were calculated with the Lewis equation (Eq. (8)). The standard NF EN 15026 (AFNOR, 2008) also proposes a direct calculation of mass transfer (h_m) coefficient ($h_m = (67 + 90\mathrm{v_{air}})\delta_{v,air}$, where $\delta_{v,air}$ is the water vapour permeability in air and v_{air} is the air velocity). For comparison, all the mass transfer coefficients h_m are presented in Figure 4. As h_m from direct calculation seems to stand out from the other values, it will be not considered. A mean value of the four other values was retained, for v_{air} = 0.5 m.s^{-1}, $h_{m,v_{air,0.5}}$=4.51 10^{-8} kg.m^{-2}.s^{-1}.Pa^{-1} and, for v_{air} = 2 m.s^{-1}, $h_{m,v_{air,2}}$=8.18 10^{-8} kg.m^{-2}.s^{-1}.Pa^{-1}.

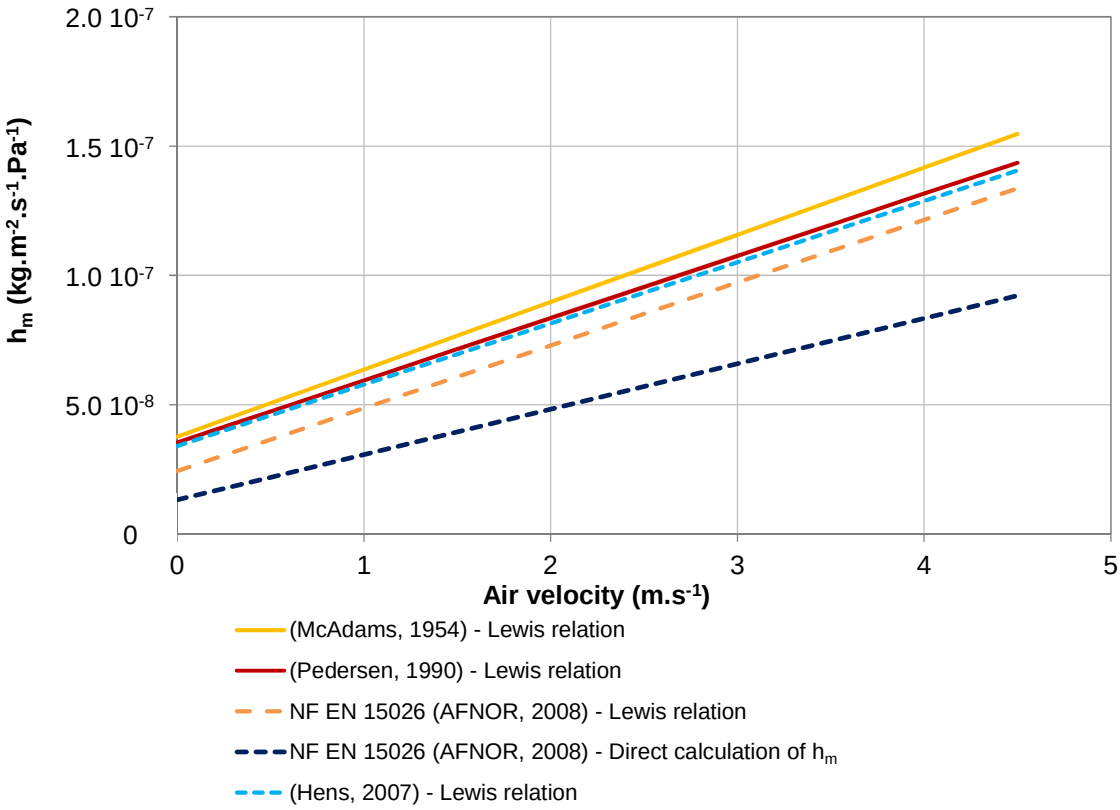

Figure 4: Calculated mass transfer coefficients h_m.

According to the standard NF EN ISO 12572 (AFNOR, 2016), the water vapour interface resistance can be neglected ($Z_{int} \approx 0$ m^2.s.Pa.kg^{-1}) when the air velocity is high enough, i.e., higher than 2 m.s^{-1}. In the case of very permeable material, the water vapour resistance of the air layer inside the cup is taken into account (Annex H of NF EN ISO 12572 (AFNOR, 2016)). So, using Eq. (6), Eq. (4) becomes Eq. (9) and the material water permeability can be deduced from Eq. (10):

$$g_v = \frac{1}{Z_{mat} + Z_{air}} \Delta p_v \quad (9)$$

$$\delta_{v,mat} = \frac{d}{\frac{\Delta p_v}{g_v} - \frac{d_{air}}{\delta_{v,air}}} \Delta p_v \quad (10)$$

where d is the material thickness (m), d_{air} is the air layer thickness (m) and $\delta_{v,air}$ is the water vapour permeability in air (kg.m^{-1}.s^{-1}.Pa^{-1}) which can be expressed by the Schirmer formula (AFNOR, 2016). We will take the value at 23°C and 1 bar, $\delta_{v,air}$=1.95 10^{-10} kg.m^{-1}.s^{-1}.Pa^{-1}.

An alternative expression, proposed in Annex G of the standard NF EN ISO 12572 (AFNOR, 2016), evaluates the water vapour resistance of the air layer Z_{air}. Two tests must then be performed: the first evaluates the total water vapour resistance $Z_{tot,1}$, Eq. (11), and the second, which contains two layers of material, evaluates the total resistance $Z_{tot,2}$, Eq. (12):

$$Z_{tot,1} = Z_{HC} + Z_{air} \quad (11)$$

$$Z_{tot,2} = 2Z_{HC} + Z_{air} \quad (12)$$

Thus, the water vapour resistance in the air layer can also be determined experimentally by Eq. (13):

$$Z_{air} = 2Z_{tot,1} - Z_{tot,2} \quad (13)$$

The permeability of a material can also be characterized by the water vapour resistance factor μ (Eq. (14)):

$$\mu = \delta_{v,air}/\delta_v \quad (14)$$

2.2.3. Capillary absorption coefficient

The capillary absorption coefficient A_w ($kg.m^{-2}.s^{-1/2}$) is used for describing capillary suction phenomena. The measurement was based on the method of Arliguie and Hornain (2007) (Figure 5). Prior to the test, the samples were dried and put into a desiccator at room temperature to reach temperature equilibrium (19±2 °C) (section 2.2). The samples were then placed in contact with water to a depth of a few millimetres. In order to ensure one-dimensional transfer, the sides were sealed with waterproof aluminium tape. The samples were then weighed regularly. Due to the fast kinetics of absorption, the weighing times were adapted to: 0, 1, 3, 5, 7, 10, 15, 20 and 30 min, 1 h and 2 h. Six samples were tested.

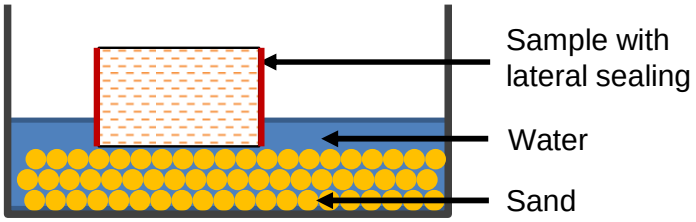

Figure 5: Sketch of the apparatus for measuring capillary absorption coefficient.

When the specific mass gain is plotted against the square root of time, the capillary absorption coefficient corresponds to the slope of the linear part of the curve. (Eq. (15)).

$$A_w = \frac{\Delta m}{A\sqrt{t}} \tag{15}$$

where Δm is the mass gain (kg), A is the area of sample surface exposed to water (m^2), and t is the time of absorption (s).

The moisture content at "free saturation" w_f was evaluated through hydrostatic weighings on 4 samples (25x10x2.5 cm^3). These samples were saturated without vacuum, i.e. the samples were only immersed in water. The moisture content at "free saturation" can be used to evaluate the liquid transfer coefficient for absorption.

3. Results and discussion

3.1. Sorption isotherm

Figure 6 compares the adsorption isotherm of hemp concrete found using different methods: a single RH step, gradual RH steps and DVS.

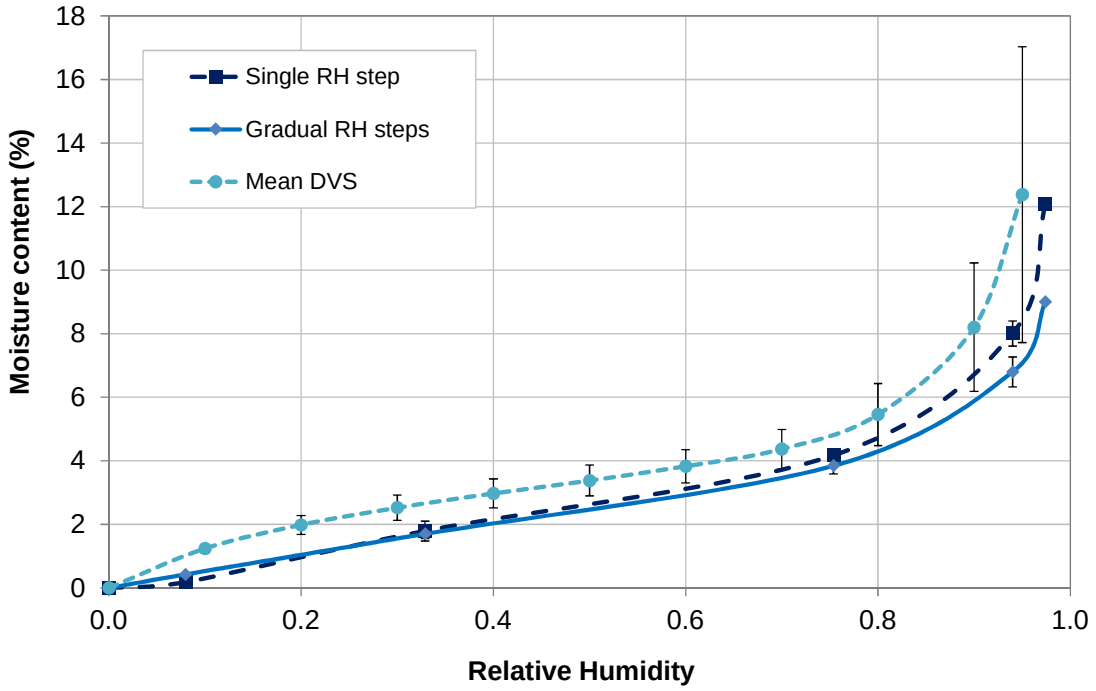

Figure 6: Adsorption isotherm measured with a single RH step equilibrium, gradual RH steps and DVS.

First, we can see that sorption isotherms with SSS have quite low dispersion, unlike the DVS measurements. In addition, the latter method works on small samples and thus the apparatus may suffer from representativeness issues. This is particularly noticeable for RH>70% where the coefficient of variation ranges from 18 to 38%.

It can be observed that the DVS measurement presents adsorption with higher moisture content over the whole RH range. Similar observations can be found in the literature: Cagnon et al. (2014) reported this on earth brick and Laborel-Prénéron (2017) on three plant aggregates. The drying procedure was different for SSS and DVS methods. The drying step in DVS permitted more precise control of the RH and temperature conditions. Therefore a possibly lower initial dry mass could lead to higher moisture content during the measurement.

Although the possible problem of representativeness may be a drawback, the DVS results had the advantage of being obtained in a shorter time, around 3.5 days, and automatically; while the SSS method with gradual RH steps lasted around 150 days and needed regular weighing operations. However the SSS methods also allowed numerous samples to be studied in parallel.

Regarding the SSS methods at low and medium humidities, the results of the two approaches were similar. For high RH, it appears that the method using a single RH step leads to a higher moisture content than the stepwise approach: for RH=94%, the moisture content was 8% in a single step against 6.8% for the stepwise approach (18% higher), and for RH=97%, the single step reached 12.1%, against 9% for the stepwise method (34% higher).

The reason for the difference of equilibrium between the two methods using the SSS (single RH step and gradual RH steps) could be linked to the specific sorption kinetics of water on cellulose-based materials or, more generally, bio-polymers. Previous studies have shown that this sorption process can be described as a fast process and a slow process occurring at the same time, with, for example, a parallel exponential kinetics (PEK) model (Hill et al., 2010; Oliver and Meinders, 2011; Popescu et al., 2015, 2016; Sharratt et al., 2011; Xie et al., 2010; Zaihan et al., 2010). In this interpretation, we can consider the sorption process as absorption since it includes both adsorption at the surface of the solid (fast process) and integration of the water molecules directly into the solid matrix (slow process): the fast process can be depicted by Fickian diffusion behaviour connected to the accessible sorption sites while the slow process may be linked to the biopolymer matrix relaxation process due to a rearrangement of the solid structure with the water molecules. At high RH (93% and 97% RH), with the single RH step method, there was a marked difference of humidity state between the initially dry samples and the environment, while this difference was smaller in the stepwise approach.

Thus, based on the Fickian diffusion interpretation, the mass gain rate was expected to be higher in the single RH step method for high RH conditions: this can be observed from the steeper slope in Figure 7. Considering the slow process, in a critical review on wood-water interactions, Tang Engelund (2013) reported that wood subjected to a higher RH step reached equilibrium more promptly. After studying the kinetics of water vapour adsorption in gluten and starch films, Oliver and Meinders (2011) suggested that the polymer matrix relaxation process can lead to a progressive rejection of water. These observations underlined the impact of the sample moisture history on the equilibrium water content and the importance of the recommended stabilization criteria, which might need to be adjusted for cellulose-based materials in order to allow for the slow rearrangement phenomena. However, very long times of stabilization induce an increased risk of mould growth on bio-sourced materials for high RH (Bui et al., 2017). Further experiments are then required to confirm these assumptions since the single RH step method is often preferred due to the time needed for this measurement.

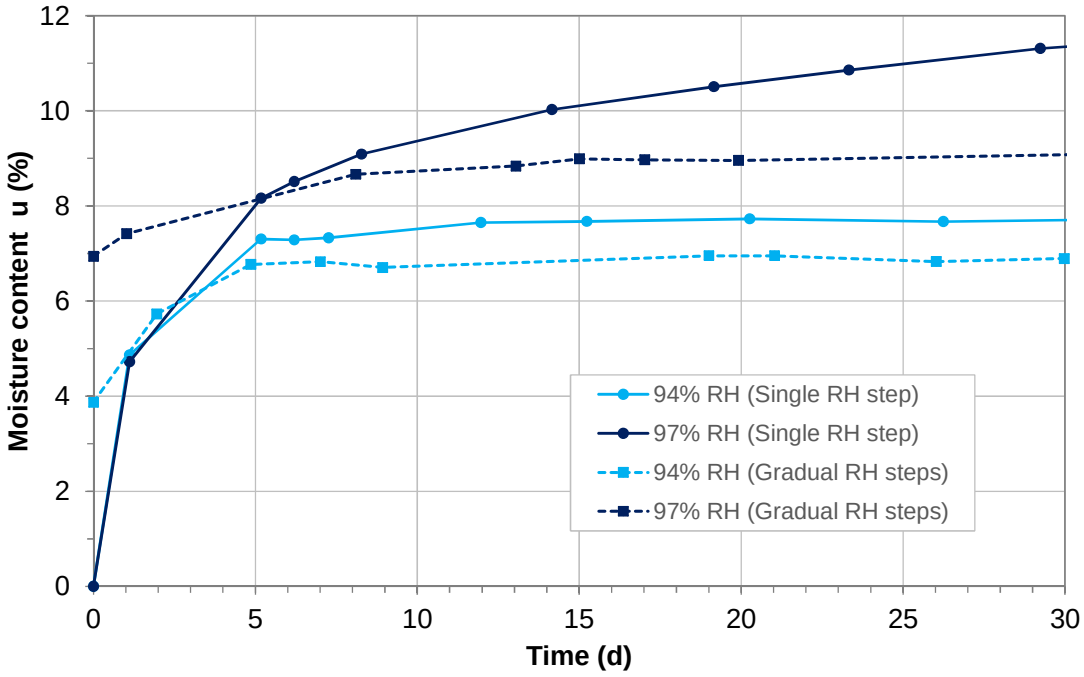

Figure 7: Typical initial sorption kinetics at RH=94% and RH=97%.

For low and medium relative humidities, our results are similar to those in the literature (Figure 8), namely close to the works of Collet et al. (2013), de Bruijn and Johansson (2013), Evrard (2008) and Rahim et al. (2016) (Figure 8). However, for high RH, i.e. for RH>90%, the moisture content is more scattered between the different references. Our material reached 9% of water content with the stepwise method and 12% with the single RH step method at 97% RH. For a similar RH condition, moisture contents found in the literature range from 10% to 44%. This result emphasizes once again the major impact of experimental parameters on the determination of equilibrium water content for high RH.

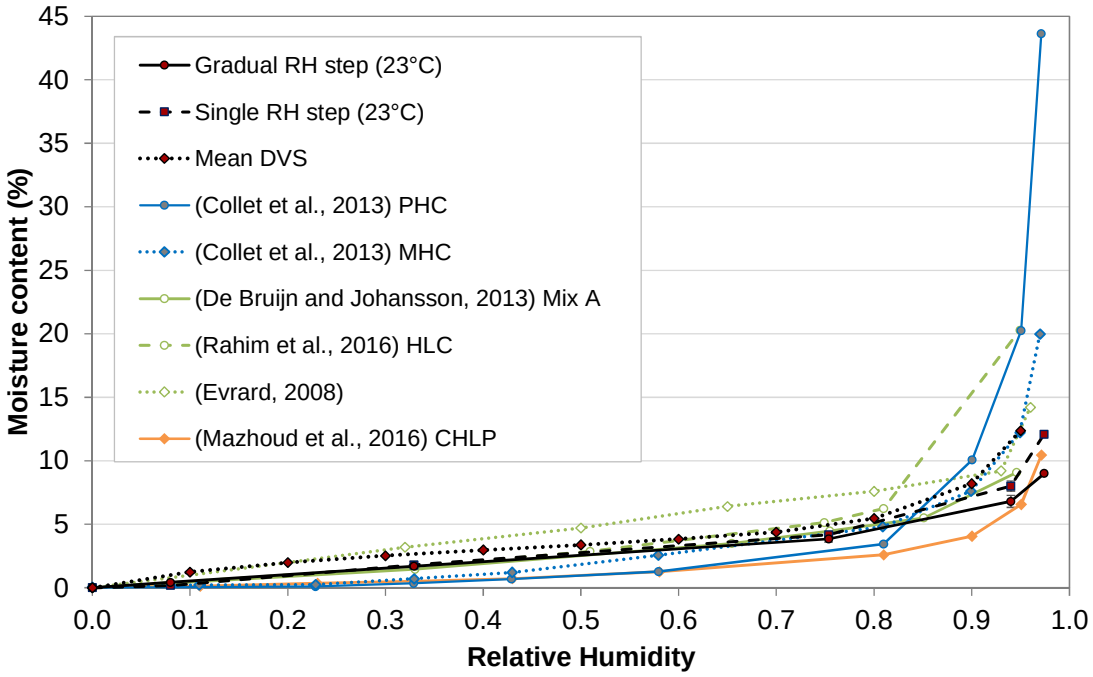

Figure 8: Adsorption isotherm measured with a single RH step equilibrium, gradual RH steps and DVS compared to a few literature references.

Desorption was also performed at 23 °C (Figure 9). As expected, a hysteresis effect occurred. Likewise, the adsorption (gradual RH steps) and desorption at 45 °C are presented in Figure 9. We can see that the experimental discrepancy is accentuated at 45 °C. As expected, the moisture content is lower than that at 23 °C.

The GAB model was used for fitting the adsorption and desorption at both 23 °C and 45 °C (Figure 9). The GAB fitting parameters are presented in Table 3.

Sorption curve	u_m	C	K
Adsorption 23 °C (Gradual RH steps)	0.0138	15.202	0.8653
Desorption 23 °C	0.0182	18.048	0.8219
Adsorption 45 °C (Gradual RH steps)	0.0129	5.0296	0.8321
Desorption 45 °C	0.0153	12.825	0.7974

Table 3: GAB fitting coefficients for adsorption and desorption at 23 °C and 45 °C

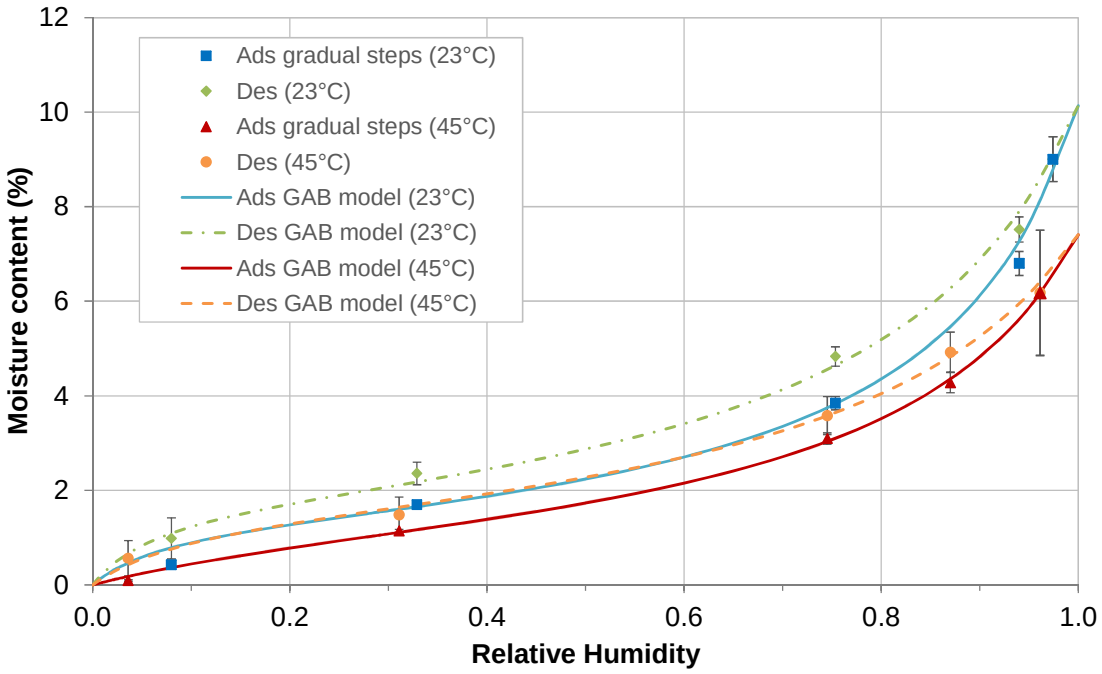

Figure 9: Adsorption (Ads) and desorption (Des) at 23 °C and 45 °C, experimental data and GAB model.

No consensus has been reached on the impact of the temperature on the sorption isotherm. The subject has been treated experimentally in the scientific literature, mainly with conventional building materials, such as concrete and hardened cement: Daïan (1988) measured the adsorption for concrete materials at 20, 35, 45 and 55 °C, as did Ishida et al. (2007) for temperatures at 20, 40 and 60 °C. Radjy et al. (2003) studied cement pastes for temperatures from 0 °C to 60 °C. All these works showed that, with higher temperature, the moisture content at equilibrium is lower even if this impact is limited. However it appears that the effect is accentuated for desorption (Ishida et al., 2007; Poyet and Charles, 2009).

Feng and Janssen (2016) focused on the gravimetric method in order to evaluate the impact of temperature on sorption. Their study dealt with three materials (aerated concrete, calcium silicate and ceramic brick). They found that the impact could be smaller than the experimental error and even observed an inconsistent tendency of the temperature impact in their

experiment. Although their study was performed on inorganic material, they noticed from the literature that the impact of the temperature could be higher on organic materials (wood and foodstuffs). The case of bio-aggregate-based building materials was also considered recently: Aït Oumeziane et al. (2016), Colinart and Glouannec (2017) and Rahim et al. (2016b) focused on hemp concrete. In addition, Colinart and Glouannec (2017), who compared an autoclaved aerated concrete, a wood fibre insulation and a hemp concrete, showed that the effect of temperature was more accentuated on organic materials than on inorganic ones.

The work of Aït Oumeziane et al. (2016) and Colinart and Glouannec (2017) relied on the Clausius-Clapeyron equation, which showed rather good agreements with experimental sorption at different temperatures. According to Brunauer (1945), the isosteric heat of sorption q_{st} (J.kg^{-1}), which corresponds to the energy released during the sorption process for a quantity of water, can be defined by the Clausius-Clapeyron relation, Eq. (16):

$$q_{st}(u) = -\frac{R}{M_w}\left[\frac{\partial \ln p_v}{\partial\left(\frac{1}{T}\right)}\right]_u \tag{16}$$

where M_w is the water molar mass (kg.mol^{-1}), p_v is the water vapour pressure (Pa) and T the temperature (K) at equilibrium with a moisture content u (kg/kg).

The integration of Eq. (16) between two states of equilibrium (pv_1, T_1) and (pv_2, T_2) for an arbitrary moisture content u gives, Eq. (17):

$$q_{st}(u) = \frac{R}{M_w}\ln\left(\frac{p_{v1}(u)}{p_{v2}(u)}\right)\left(\frac{T_1 T_2}{T_1 - T_2}\right) \tag{17}$$

Therefore, knowing the sorption isotherms at two temperatures allowed the isosteric heat of sorption to be calculated as a function of the moisture content. Nevertheless, a reciprocal

sorption model was adopted as there was not enough experimental data. As presented by Poyet and Charles (2009), the reciprocal GAB relation gives, for a temperature T_i (Eq. (18)):

$$p_{vi}(u) = \frac{p_s(T_i)}{2K_i(1-C_i)}\left[\alpha_i - \sqrt{\alpha_i^2 - 4(1-C_i)}\right] \quad (18)$$

where $\alpha_i = 2 + \left[\frac{u_{mi}}{u} - 1\right]C$; K_i, C_i and u_{mi} are the three parameters used to characterize a GAB sorption curve.

Combining Eqs. (17) and (18) gives an evaluation of the isosteric heat of sorption q_{st}. The result of q_{st} as a function of the moisture content is presented in Figure 10.

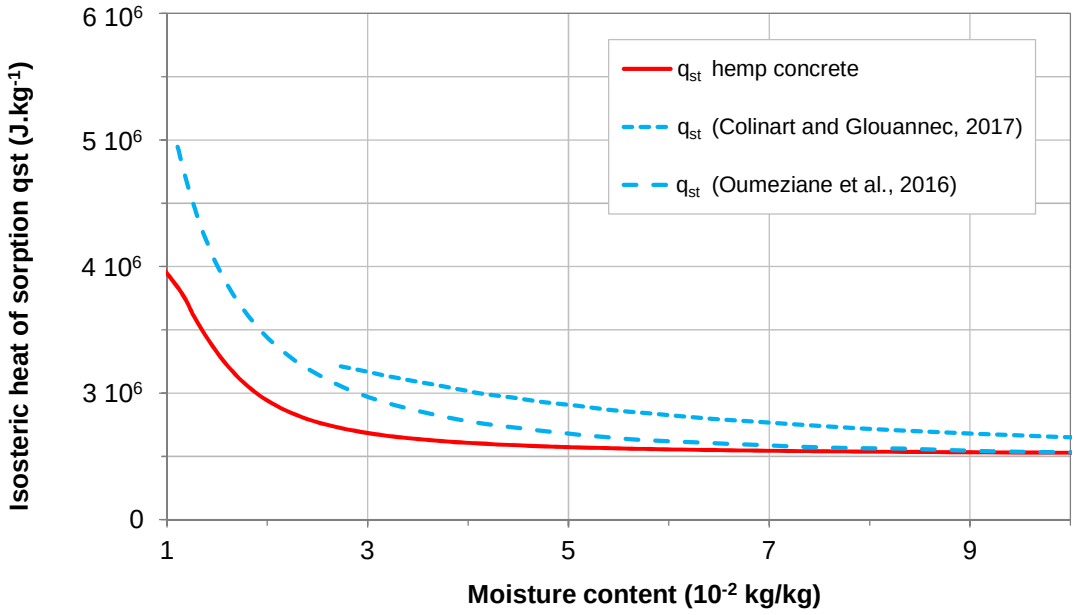

Figure 10: Calculated heat of sorption.

With the isosteric heat of sorption, it is then possible to evaluate the sorption isotherm at a given temperature T (Eq. (19))

$$RH(T,u) = RH\left(T_{ref},u\right)\frac{p_{v,\mathrm{sat}}\left(T_{ref}\right)}{p_{v,sat}(T)}\, e^{q_{st}(u)\frac{M_w}{R}\frac{(T-T_{ref})}{T\cdot T_{ref}}} \quad (19)$$

This model will be applied to evaluate the impact of the temperature on the heat and moisture transfers by a numerical approach at wall scale.

3.2. Water vapour permeability

Table 4 sums up the apparent water vapour permeability $\delta_{v,app}$ and the apparent water vapour resistance coefficient μ_{app} deduced from four experimental campaigns that varied the method (dry or wet), the air velocity on the top surface of the cup (0.5 or 2 $m.s^{-1}$) and the thickness of the sample (5 or 8 cm).

Method	Air velocity ($m.s^{-1}$)	Sample thickness (cm)	$\delta_{v,app} = \frac{d}{Z_{app}}$ ($kg.m^{-1}.s^{-1}.Pa^{-1}$)	$\mu_{app} = \frac{\delta_{v,air}}{\delta_{v,app}}$
Dry cup	0.5	5	$7.70\ 10^{-11} \pm 1.37\ 10^{-11}$	2.59 ± 0.42
	2	5	$8.31\ 10^{-11} \pm 5.14\ 10^{-12}$	2.36 ± 0.14
		8	$9.61\ 10^{-11} \pm 1.03\ 10^{-11}$	2.05 ± 0.22
Wet cup		5	$1.13\ 10^{-10} \pm 2.20\ 10^{-11}$	1.77 ± 0.36

Table 4: Apparent water vapour permeability $\delta_{v,app}$ and water vapour resistance coefficient μ_{app} for different sets of measurements

Table 4 shows the influence of the different experimental parameters on the assessment of the apparent water vapour permeability. As expected, the apparent permeability is higher with the wet cup than with the dry cup, due to additional liquid transfer through the sample. A lower velocity of the air on the top surface of the cup induces an additional resistance to the water vapour transfer and a consequent reduction of the apparent water vapour permeability. Finally, different sample thicknesses lead to distinct values of apparent water vapour permeability, highlighting the need to evaluate the water vapour resistances of the air and interfaces (inside and outside the cup) and take them into account for an accurate determination of the water vapour permeability of the hemp concrete under study. This is done in Table 5, which gathers together the results of water vapour permeabilities, δ_v, and water vapour resistance factors, μ, while detailing the air, and the inside and outside interface

water vapour resistances, and using different methods of calculation. The calculation methods come from NF EN ISO 12572 Annex G (AFNOR, 2016) (Eq. (10)), NF EN ISO 12572 Annex H (AFNOR, 2016) (Eqs. (11) and (12)) or consider the interface resistances inside the cup and/or outside the cup as the inverse function of the mass transfer coefficient, which itself relies on the Lewis equation as detailed in the Methods section.

v_{air} = 0.5 m.s^{-1}	Z_{air}	$Z_{int, in}$	$Z_{int, out}$	$\delta_{v,mat}$	μ
	(m^2.s.Pa.kg^{-1})			(kg.m^{-1}.s^{-1}.Pa^{-1})	
NF EN ISO 12572 Annex G	$9.01\ 10^7 \pm 5.32\ 10^6$	-	-	$8.63\ 10^{-11} \pm 1.39\ 10^{-11}$	2.30 ± 0.34
Calculation considering the air layer and the interface resistances - Dry cup	$9.01\ 10^7 \pm 5.32\ 10^6$	-	$2.22\ 10^7$	$8.97\ 10^{-11} \pm 1.51\ 10^{-11}$	2.22 ± 0.34
	$9.01\ 10^7 \pm 5.32\ 10^6$	$3.05\ 10^7$	-	$9.10\ 10^{-10} \pm 1.56\ 10^{-11}$	2.18 ± 0.34
	$9.01\ 10^7 \pm 5.32\ 10^6$	$3.05\ 10^7$	$2.22\ 10^7$	$9.48\ 10^{-11} \pm 1.71\ 10^{-11}$	2.10 ± 0.35
v_{air} = 2 m.s^{-1}	Z_{air}	$Z_{int, in}$	$Z_{int, out}$	$\delta_{v,mat}$	μ
	(m^2.s.Pa.kg^{-1})			(kg.m^{-1}.s^{-1}.Pa^{-1})	
NF EN ISO 12572 Annex G	$9.01\ 10^7 \pm 5.32\ 10^6$	-	-	$9.67\ 10^{-11} \pm 6.35\ 10^{-12}$	2.02 ± 0.13
NF EN ISO 12572 Annex H	$2.35\ 10^8 \pm 2.28\ 10^8$		-	$1.31\ 10^{-10}$	1.49
Calculation considering the air layer and the interface resistances - Dry cup	$9.01\ 10^7 \pm 5.32\ 10^6$	-	$1.22\ 10^7$	$9.89\ 10^{-11} \pm 6.64\ 10^{-12}$	1.98 ± 0.13
	$9.01\ 10^7 \pm 5.32\ 10^6$	$3.05\ 10^7$	-	$1.02\ 10^{-10} \pm 7.10\ 10^{-12}$	1.91 ± 0.13
	$9.01\ 10^7 \pm 5.32\ 10^6$	$3.05\ 10^7$	$1.22\ 10^7$	$1.05\ 10^{-10} \pm 7.44\ 10^{-12}$	1.87 ± 0.13

Table 5: Water vapour permeabilities δ_v, and water vapour resistance factors μ, with the air/interface resistance details, according to different methods of calculation (5 cm sample, v_{air} = 2 m.s^{-1} and v_{air} = 0.5 m.s^{-1})

Depending on the method of calculation, the water vapour permeability value of the hemp concrete ranges from $8.63\ 10^{-11}$ to $1.31\ 10^{-10}$ kg.m^{-1}.s^{-1}.Pa^{-1} (Table 5). When the air layer is neglected, the apparent water vapour permeability is around $8.31\ 10^{-11}$ kg.m^{-1}.s^{-1}.Pa^{-1} (Table 4), 14% lower than the value given in NF EN ISO 12572 Annex G. Looking at the different

values measured when the air velocity was 2 $m.s^{-1}$, we can see that the impact of the outside interface resistance is indeed limited, with an increase of around 2% on the water vapour permeability, compared to the value in NF EN ISO 12572 Annex G. The inside interface resistance has a slightly higher impact, with an increase of around 6%.

The method proposed in Annex H of standard NF EN ISO 12572 leads to a particularly high value of water vapour permeability: 1.31 10^{-10} $kg.m^{-1}.s^{-1}.Pa^{-1}$, which is 31% higher than calculated in NF EN ISO 12572 Annex G. It can be noted that the standard estimation of the air layer water vapour resistance (Eq. (10)), according to annex G, would lead to $Z_{air,Annex\ G}$ =8.4 10^{7} $m^2.s.Pa.kg^{-1}$ while the method of Annex H of NF EN ISO 12572 leads to $Z_{air,\ Annex\ H}$=2.4 10^{8} $m^2.s.Pa.kg^{-1}$, 2.3 times higher. This can suggest that Eq. (10) underestimates the air permeability when applied to an air layer, or that the value found by Eqs. (11) and (12) may also take other water vapour resistances into account, such as interface water vapour resistance inside or outside the cup.

Comparing the air velocities, we see that decreasing the air velocity from 2 $m.s^{-1}$ to 0.5 $m.s^{-1}$ decreases the apparent water vapour permeability by around 10%.

The “wet cup” measurement gives a value of 1.42 10^{-10} $kg.m^{-1}.s^{-1}.Pa^{-1}$ according to the calculation of standard NF EN ISO 12572 Annex G (μ=1.43).

The NF EN ISO 12572 Annex H calculation can also be obtained with Eqs. (20) and (21), considering the general expression of the apparent water vapour resistances at 2 $m.s^{-1}$ and 0.5 $m.s^{-1}$ with 2 layers of material:

$$Z_{app.2,\ 2\ m.s^{-1}} = Z_{int,\ 2\ m.s^{-1}} + 2Z_{mat} + Z_{air} \quad (20)$$

$$Z_{app.2,\ 0.5\ m.s^{-1}} = Z_{int,\ 0.5\ m.s^{-1}} + 2Z_{mat} + Z_{air} \quad (21)$$

Subtracting Eq. (21) from Eq. (20) gives $\Delta Z_{int} = Z_{int,\ 0.5\ m.s^{-1}} - Z_{int,\ 2\ m.s^{-1}}$= 5 10^7 (m^2.s.Pa.kg^{-1}) experimentally. In contrast, the theoretical difference of interface water vapour resistances is shown in Table 6 with the details of the calculations. They are based on the values of NF EN 15026 (AFNOR, 2008), Hens et al. (2007), McAdams (1954) and Pedersen (1990). Thus the experimental results show that the air velocity may have a higher impact on the interface air resistance than expected.

	Theoretical				Experimental
v_{air} ($m.s^{-1}$)	h_c ($W.m^{-2}.K^{-1}$)	h_m ($kg.m^{-2}.s^{-1}.Pa^{-1}$)	$Z_{int,th}$ ($m^2.s.Pa.kg^{-1}$)	$\Delta Z_{int,th}$ ($m^2.s.Pa.kg^{-1}$)	$\Delta Z_{int,expe}$ ($m^2.s.Pa.kg^{-1}$)
0.5	7.4	4.51 10^{-8}	2.3 10^7	1 10^7 ± 3.1 10^6	5 10^7 ± 2.3 10^7
2	13.5	8.18 10^{-8}	1.3 10^7		

Table 6: Calculated $\Delta Z_{int,th}$ according to NF EN ISO 12572 Annex H and experimental value $\Delta Z_{int,expe}$

Perfect control of the value and the homogeneity of the air velocity at the top of the cup is quite difficult to obtain in a standard climatic chamber. Vololonirina and Perrin (2016) warned that it can be difficult to apply Lewis analogy because of lack of control of the air flow.

Nevertheless, we note that, even with a more extreme theoretical difference of the air velocity, we still obtain a $\Delta Z_{int,th}$ that is smaller than the experimental one: for instance, if we choose v_{low} = 0.25 $m.s^{-1}$ and v_{high} = 5 $m.s^{-1}$, ΔZ_{int} = 1.9 10^7 m^2.s.Pa.kg^{-1}< $\Delta Z_{int,expe}$.

To conclude on this results analysis, the interface resistance inside and outside impacts the value of the water vapour permeability by about 10%. Decreasing the air velocity from 2 $m.s^{-1}$ to 0.5 $m.s^{-1}$ also increases the final value by about 10%. Here, confronting the two extreme approaches, i.e. the standard calculation at low air velocity and the calculation considering all

surface resistances at high air velocity, gives a difference of 22% on the value of the water vapour permeability. So, for highly permeable building materials such as hemp concrete, the water vapour measurement method is experimentally sensitive to the air velocity and to the evaluation of the air resistance above the cup, and to the air layer and the surface resistance inside the cup.

Whatever the approach, the measured water vapour permeabilities appear to be higher than most of the literature values: Rahim et al. (2016b) found 2.23 10^{-11} $kg.m^{-1}.s^{-1}.Pa^{-1}$ (μ=8.8) when considering the interface and air layer resistances. Evrard (2008) and Strandberg-de Bruijn and Johansson (2014) measured 4.0 10^{-11} $kg.m^{-1}.s^{-1}.Pa^{-1}$ (μ=4.9) and 3.6-3.9 10^{-11} $kg.m^{-1}.s^{-1}.Pa^{-1}$ respectively (μ=5-5.5), taking the air layer into account. Note that the relative humidities used in the latter study were 33.1% and 54.4%. Thus, the water vapour permeability measured from a standard dry cup might be lower. Collet et al. (2013) found 2.51 10^{-11} $kg.m^{-1}.s^{-1}.Pa^{-1}$ (μ=7.8) for a precast hemp concrete without considering the air layer. Only Walker and Pavía (2014) reported higher water vapour permeability, of 3.99 10^{-10} $kg.m^{-1}.s^{-1}.Pa^{-1}$.

A high level of discrepancy can be noted in the literature values. Different parameters contribute to this dispersion: the design of the hemp concrete itself, the method of calculation of the water vapour resistance of the air layer inside and outside the cup and the experimental protocol parameters (among which the most impacting would be the air flux direction, the sealing material and method, the nature of the desiccant or saturated salt solution and the area and thickness of the material). Thus, a round-robin test could be interesting for setting a protocol suitable for highly permeable material with, for example, a multi-parameter study among different laboratories from the same batch of material.

Despite the discrepancy of the water vapour permeability in the literature, all these values present high permeabilities and confirm the potential of hemp concrete as a hygroscopic material. For comparison, the water vapour permeability of concrete (ρ=2250 kg.m^{-3}), light weight aggregate concrete (ρ=1500 kg.m^{-3}), brick (ρ=1600 kg.m^{-3}) and cellular concrete (ρ=500 kg.m^{-3}) are respectively 5 10^{-12} (μ=39), 1 10^{-11} (μ=20), 3 10^{-11} (μ=7) and 7 10^{-11} (μ=3) (kg.m^{-1}.s^{-1}.Pa^{-1}) (Rode et al., 2005).

3.3. Liquid transfer coefficient

Figure 11 presents the results for capillary absorption, i.e. the linear part of the curve presenting the mass variation as a function of the square root of the time, which begins after 1 min of testing and stops when the water reaches the top of the sample. Before 1 min, there is a change of slope, indicating that the mass increase is not ruled by capillary absorption only. The mean water absorption coefficient is A_w =0.14 ± 0.01 kg.m^{-2}.s$^{-1/2}$. This value is higher than the value measured by Evrard (2008) and Walker and Pavía (2014): 0.07 kg.m^{-2}.s$^{-1/2}$ but it is in the same range as for the hemp concrete studied by de Bruijn et al. (2009), who measured 0.15 kg.m^{-2}.s$^{-1/2}$.

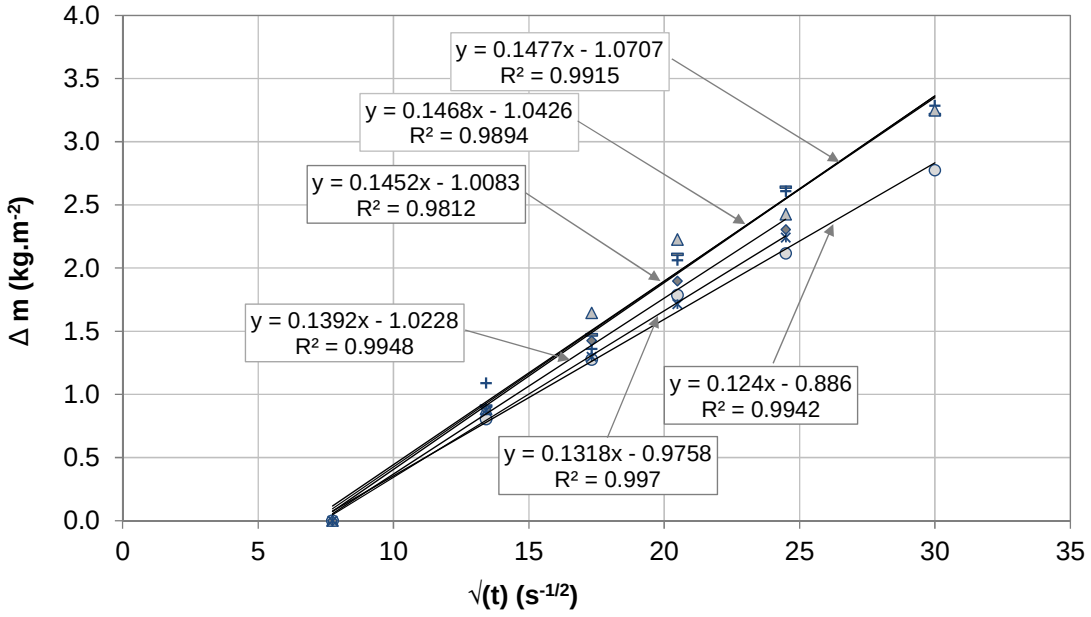

Figure 11: Water mass absorption as a function of square root of time.

Künzel (1995) expressed the liquid transfer coefficient for absorption D_w ($m^2.s^{-1}$):

$$D_w = 3.8\left(\frac{A_w}{w_f}\right)^2 1000^{\frac{w}{w_f}-1} \quad (22)$$

where A_w is the liquid absorption coefficient, w is the moisture content ($kg.m^{-3}$) and w_f is the moisture content at free saturation ($kg.m^{-3}$). With A_w = 0.14 $kg.m^{-2}.s^{-1/2}$ and the moisture content at free saturation w_f = 541 $kg.m^{-3}$, we find $D_{w,cap.\ abs.,72\%}$ = 3.2 10^{-10} $m^2.s^{-1}$

According to Künzel (1995), the wet-cup method can help with determining the liquid transfer coefficient in the hygroscopic region $D_{w,wet\text{-}cup}$ ($m^2.s^{-1}$). As can be observed in the literature, the apparent water vapour permeability increases with RH; for instance Collet et al. (2013) obtained value from 1.7 10^{-11} kg m^{-1} s^{-1} Pa^{-1} at low humidity and up to 1.3 10^{-11} kg m^{-1} s^{-1} Pa^{-1} at high humidity. As explained previously, increasing the RH will increase the part played by liquid transfer in the apparent water vapour permeability. Thus, Künzel (1995)

separated the contribution of the water vapour only (referred as μ_0), identified from the value at low RH, from the apparent measurement, thus isolating the liquid contribution, Eq. 23:

$$D_{w,wet-cup} = \frac{p_{v,sat}\,\delta_{v,air}}{\xi_{\mathrm{RH}}}\left(\frac{1}{\mu^*}-\frac{1}{\mu_0}\right) \quad (23)$$

where $p_{v,sat}$ is the saturated vapour pressure (Pa), $\delta_{v,air}$ is the water vapour permeability in air (kg m^{-1} s^{-1} Pa^{-1}), ξ_{RH} is the moisture capacity ($\xi_{\mathrm{RH}} = dw/d\mathrm{RH}$ in kg.m^{-3}), μ^* is the apparent water vapour resistance factor ($\mu^*=\mu_{\text{wet cup}}$=1.4 in this case) and μ_0 is the water vapour resistance factor in dry conditions (μ_0=2.0).

The calculated liquid transfer coefficient at RH=72%, the average RH between the two conditions of 50% and 94% RH, is $D_{w,wet-cup,72\%}$=3.8 10^{-9} m^2.s^{-1}, which is almost 12 times the value found with capillary absorption.

4. Conclusion

This paper has characterized the hygric properties of a precast hemp concrete.

The adsorption and desorption of the hemp concrete was measured at 23 °C and 45 °C. For the standard measurement at 23 °C, different methods were confronted: two methods with saturated salt solutions (SSS) (single RH step method and stepwise method) and a DVS were used. Differences were observed: for all RH, the DVS moisture contents were higher than the other measurements, and the single RH step method led to higher moisture content than the stepwise approach for high RH. For DVS measurements, such observations have been made previously in the literature and could be linked to distinct drying procedures for SSS and DVS methods. For the two SSS methods, the difference could be explained by the specific water vapour sorption process on cellulose-based materials. Two different sorption mechanisms

coexist: a fast process linked to the sorption sites on the solid and a slow process linked to the rearrangement of the solid matrix. Thus the impact of the method needs to be clarified since the single RH step method is often adopted in order to reduce the experimental time.

The measurement of the isotherm at two temperatures allows the impact of temperature on sorption to be evaluated through an isosteric heat of sorption and GAB model. This temperature-dependent model will be used to evaluate the impact of the temperature on the heat and moisture transfers with numerical studies.

The water vapour permeability was measured with the dry and wet cup tests, based on the standard NF EN ISO 12572 (AFNOR, 2016). Two thicknesses of material and two air velocities were tested, together with different methods of calculation, which either took into account or ignored the several additional water vapour resistances (air layer, inside interface resistance, outside interface resistance). The interface resistance inside and outside was found to impact the value of the water vapour permeability by about 10%. Decreasing the air velocity from 2 $m.s^{-1}$ to 0.5 $m.s^{-1}$ also increased the final value by about 10%. Here, confronting the two extreme approaches, i.e. standard calculation at low air velocity and calculation considering all surface resistances at high air velocity, gave a difference of 22% on the value of the water vapour permeability. The method proposed by NF EN ISO 12572 Annex H was also tested but led to a water vapour permeability 31% higher than the NF EN ISO 12572 Annex G calculation, i.e. the calculation considering the air layer water vapour resistance with Fickian diffusion. The water vapour measurement protocol appeared to be sensitive to several factors in the case of very permeable materials such as hemp concrete.

The capillary absorption coefficient was measured with capillary uptake tests and showed good agreement with the literature. The liquid transfer coefficient for absorption presented by Künzel (1995) was also evaluated and appeared to be 12 times lower than the evaluation based on wet cup water vapour permeability (Künzel, 1995).

This paper completes the thermal characterization carried out in the first of this pair of articles (Seng et al., 2018) and highlights the sensitivity of the results to the selected experimental methods. An inter-laboratory round robin test based on the same bio-sourced materials is now needed for a comprehensive comparison of the different protocols and to draw up recommendations for the accurate hygrothermal characterization of such materials.

The hygrothermal properties of a precast hemp concrete will be used with the thermal properties measured in the first paper of this series (Seng et al., 2018) as input for heat and moisture transfer modelling (Seng et al., 2017). These numerical results will then be confronted with measurements made on a wall-scale setup (Vu et al., 2015). A sensitivity analysis of the model should allow the most influential hygrothermal properties to be identified.

5. Acknowledgments

The authors would like to acknowledge the SEAC company for providing the materials for this study and the scientific project neOCampus, led by Paul Sabatier University Toulouse III, which supports this work.

6. References

AFNOR, 2016. NF EN ISO 12572 - Hygrothermal performance of building materials and products — Determination of water vapour transmission properties — Cup method.

AFNOR, 2013. NF EN ISO 12571 - Hygrothermal performance of building materials and products — Determination of hygroscopic sorption properties.

AFNOR, 2008. NF EN 15026 - Hygrothermal performance of building components and building elements - Assessment of moisture transfer by numerical simulation.

AFNOR, 2001. NF EN ISO 12572 - Hygrothermal performance of building materials and products — Determination of water vapour transmission properties.

Aït Oumeziane, Y., Moissette, S., Bart, M., Lanos, C., 2016. Influence of temperature on sorption process in hemp concrete. Construction and Building Materials 106, 600–607.

Anderson, R.B., 1946. Modifications of the Brunauer, Emmett and Teller Equation. Journal of the American Chemical Society 68, 686–691.

Arliguie, G., Hornain, H., 2007. GranDuBé -Grandeur associées à la durabilité des Bétons. Presses de l'école nationale des Ponts et chaussées.

Brunauer, S., 1945. The adsorption of gases and vapors, Physical Adsorption, Princeton University Press. ed.

Bui, R., Labat, M., Aubert, J.-E., 2017. Comparison of the Saturated Salt Solution and the Dynamic Vapor Sorption techniques based on the measured sorption isotherm of barley straw. Construction and Building Materials 141, 140–151.

Cagnon, H., Aubert, J.E., Coutand, M., Magniont, C., 2014. Hygrothermal properties of earth bricks. Energy and Buildings 80, 208–217.

Colinart, T., Glouannec, P., 2017. Temperature dependence of sorption isotherm of hygroscopic building materials. Part 1: Experimental evidence and modeling. Energy and Buildings 139, 360–370.

Collet, F., Chamoin, J., Pretot, S., Lanos, C., 2013. Comparison of the hygric behaviour of three hemp concretes. Energy and Buildings 62, 294–303.

Daïan, J.-F., 1988. Condensation and isothermal water transfer in cement mortar Part I - Pore size distribution, equilibrium water condensation and imbibition. Transport in Porous Media 3, 563–589.

de Bruijn, P., Johansson, P., 2013. Moisture fixation and thermal properties of lime–hemp concrete. Construction and Building Materials 47, 1235–1242.

de Bruijn, P.B., Jeppsson, K.-H., Sandin, K., Nilsson, C., 2009. Mechanical properties of lime–hemp concrete containing shives and fibres. Biosystems Engineering 103, 474–479.

Dinh, T.M., Magniont, C., Coutand, M., Escadeillas, G., 2015. Hemp concrete using innovative pozzolanic binder. Presented at the First International Conference on Bio-based Building Materials.

Engelund, E.T., Thygesen, L.G., Svensson, S., Hill, C.A.S., 2013. A critical discussion of the physics of wood–water interactions. Wood Sci Technol 47, 141–161.
Escadeillas, G., Oms, C., Magniont, C., De, C.P., 2010. Binder composition, useful for forming construction materials, comprises natural lime binder, metakaolin binder, and binder of an adjuvant comprising shrinkage reducer, water repellent hardener. FR2946641 (A1).
Evrard, A., 2008. Transient hygrothermal behaviour of Lime-Hemp Materials (Ph.D. thesis). Université Catholique de Louvain.
Feng, C., Janssen, H., 2016. Hygric properties of porous building materials (II): Analysis of temperature influence. Building and Environment 99, 107–118.
Feng, C., Janssen, H., Feng, Y., Meng, Q., 2015. Hygric properties of porous building materials: Analysis of measurement repeatability and reproducibility. Building and Environment 85, 160–172.
Gazagnes, E., Magniont, C., Escadeillas, G., 2010. Composite material for construction comprising hemp stems. FR2946640 (A1) Synopsis of correspond document EP2263985 (A1).
Hens, H.L.S.C., Mukhopadhyaya, P., Kumaran, M., Dean, S.W., 2007. Modeling the Heat, Air, and Moisture Response of Building Envelopes: What Material Properties are Needed, How Trustful Are the Predictions? Journal of ASTM International.
Hill, C.A.S., Norton, A.J., Newman, G., 2010. The water vapour sorption properties of Sitka spruce determined using a dynamic vapour sorption apparatus. Wood Science and Technology 44, 497–514.
Ishida, T., Maekawa, K., Kishi, T., 2007. Enhanced modeling of moisture equilibrium and transport in cementitious materials under arbitrary temperature and relative humidity history. Cement and Concrete Research 37, 565–578.
Künzel, H.M., 1995. Simultaneous Heat and Moisture Transport in Building Components - One- and two-dimensionnal calculation using simple parameters (Ph.D. thesis). Fraunhofer Institute of Building Physics, Stuttgart, Germany.
Laborel-Prénéron, A., 2017. Formulation and characterization of unfired clay bricks with plant aggregates (Ph.D. thesis). Université Toulouse 3 Paul Sabatier, Toulouse, France.
Latif, E., Lawrence, M., Shea, A., Walker, P., 2015. Moisture buffer potential of experimental wall assemblies incorporating formulated hemp-lime. Building and Environment 93, Part 2, 199–209.
Magniont, C., Escadeillas, G., Coutand, M., Oms-Multon, C., 2012. Use of plant aggregates in building ecomaterials. European Journal of Environmental and Civil Engineering 16, 17–33.
Mazhoud, B., Collet, F., Pretot, S., Chamoin, J., 2016. Hygric and thermal properties of hemp-lime plasters. Building and Environment 96, 206–216.
McAdams, W.H., 1954. Heat Transmission, (3rd ed.). ed. McGraw-Hill, New York.
Oliver, L., Meinders, M.B.J., 2011. Dynamic water vapour sorption in gluten and starch films. Journal of Cereal Science 54, 409–416.
Pedersen, C.R., 1990. Combined Heat and Moisture Transfer in Building Constructions (Ph.D. thesis). Thermal Insulation Laboratory, Technical University of Denmark.
Peñaloza, D., Erlandsson, M., Falk, A., 2016. Exploring the climate impact effects of increased use of bio-based materials in buildings. Construction and Building Materials 125, 219–226.
Popescu, C.-M., Hill, C.A.S., Anthony, R., Ormondroyd, G., Curling, S., 2015. Equilibrium and dynamic vapour water sorption properties of biochar derived from apple wood. Polymer Degradation and Stability 111, 263–268.

Popescu, C.-M., Hill, C.A.S., Kennedy, C., 2016. Variation in the sorption properties of historic parchment evaluated by dynamic water vapour sorption. Journal of Cultural Heritage 17, 87–94.

Poyet, S., Charles, S., 2009. Temperature dependence of the sorption isotherms of cement-based materials: Heat of sorption and Clausius–Clapeyron formula. Cement and Concrete Research 39, 1060–1067.

Radjy, F., Sellevold, E.J., Hansen, K.K., 2003. Isosteric vapor-pressure-temperature data for water sorption in hardened cement paste : enthalpy, entropy and sorption isotherms at diffrent temperatures (Report No. Report BYG DTU R-057). Technical University of Denmark.

Rahim, M., Douzane, O., Tran Le, A.D., Promis, G., Langlet, T., 2016a. Characterization and comparison of hygric properties of rape straw concrete and hemp concrete. Construction and Building Materials 102, Part 1, 679–687.

Rahim, M., Tran Le, A.D., Douzane, O., Promis, G., Langlet, T., 2016b. Numerical investigation of the effect of non-isotherme sorption characteristics on hygrothermal behavior of two bio-based building walls. Journal of Building Engineering 7, 263–272.

Rode, C., Peuhkuri, R.H., Mortensen, L.H., Hansen, K.K., Time, B., Gustavsen, A., Ojanen, T., Ahonen, J., Svennberg, K., Arfvidsson, J., Harderup, L.-E., 2005. Moisture buffering of building materials (report BYG-DTU No. ISSN 1601 – 2917). Technical University of Denmark, Department of Civil Engineering.

Roels, S., Carmeliet, J., Hens, H., Adan, O., Brocken, H., Cerny, R., Pavlik, Z., Ellis, A.T., Hall, C., Kumaran, K., Pel, L., Plagge, R., 2004. A Comparison of Different Techniques to Quantify Moisture Content Profiles in Porous Building Materials. Journal of Thermal Envelope and Building Science 262–276.

Seng, B., Lorente, S., Magniont, C., 2017. Scale analysis of heat and moisture transfer through bio-based materials — Application to hemp concrete. Energy and Buildings 155, 546–558.

Seng, B., Magniont, C., Lorente, S., 2018. Characterization of a precast hemp concrete. Part I: Physical and thermal properties. Journal of Building Engineering. doi.org/10.1016/j.jobe.2018.07.016.

Sharratt, V., Hill, C.A.S., Zaihan, J., Kint, D.P.R., 2011. The influence of photodegradation and weathering on the water vapour sorption kinetic behaviour of scots pine earlywood and latewood. Polymer Degradation and Stability 96, 1210–1218.

Strandberg-de Bruijn, P., Johansson, P., 2014. Moisture transport properties of lime–hemp concrete determined over the complete moisture range. Biosystems Engineering 122, 31–41.

Surface Measurement Systems, 2000. DVS Manual. London.

Vololonirina, O., Coutand, M., Perrin, B., 2014. Characterization of hygrothermal properties of wood-based products – Impact of moisture content and temperature. Construction and Building Materials 63, 223–233.

Vololonirina, O., Perrin, B., 2016. Inquiries into the measurement of vapour permeability of permeable materials. Construction and Building Materials 102, Part 1, 338–348.

Vu, T.L., Spagnol, S., Magniont, C., 2015. Experimental study of the hygrothermal behaviour of hemp shives-based precast blocks at material and wall scales. Proceedings of the First International Conference on Bio-based Building Materials (ICBBM), Clermont-Ferrand, France.

Walker, R., Pavía, S., 2014. Moisture transfer and thermal properties of hemp–lime concretes. Construction and Building Materials 64, 270–276.

Xie, Y., Hill, C.A.S., Xiao, Z., Jalaludin, Z., Militz, H., Mai, C., 2010. Water vapor sorption kinetics of wood modified with glutaraldehyde. Journal of Applied Polymer Science.

Zaihan, J., Hill, C.A.S., Curling, S., Hashim, W.S., Hamdan, H., 2010. The kinetics of water vapour sorption: analysis using parallel exponential kinetics model on six Malaysian hardwoods. Journal of Tropical Forest Science 22, 107–117.